Topological phase transition in the commensurate multifrequency Floquet Su-Schrieffer-Heeger model

Sam Olin* and Wei-Cheng Lee†
Department of Physics, Applied Physics, and Astronomy, Binghamton University, Binghamton, New York 13902, USA

(Received 21 October 2022; revised 2 January 2023; accepted 23 February 2023; published 22 March 2023)

Recently, Floquet systems have attracted a great deal of interest as they offer the unprecedented ability to engineer topological states through the tuning of an external time-periodic drive. Consequentially, seeking new driving protocols that allow for more exotic topological phases and transitions becomes imperative for the Floquet engineer. In this paper, we study the Su-Schrieffer-Heeger model driven by two time-dependent periodic sources with commensurate frequencies and an amplitude modulation. Imposing more than one driving frequency allows us to realize even more exotic topological phases resulting from new couplings appearing in the Fourier space representation. Moreover, we find an experimentally practical method for sweeping the system through a topological phase transition by varying the amplitude mixture of the commensurate sources. We employ the local Chern marker, a real-space representation of the Chern number, to simulate topological phase diagrams of the two-drive Floquet Hamiltonian in a variety of driving cases.

DOI: 10.1103/PhysRevB.107.094310

I. INTRODUCTION

Topology has signaled a shift in modern condensed-matter research since the emergence of the quantum Hall effect [1]. Many systems with desirable physical behaviors are now known to have an underlying nontrivial topological classification [2–5]. These systems are promising platforms to potentially revolutionize technology as we approach the limit of traditional semiconductor-based devices [6]. One idea is to design electronics using the robust conducting edge states of topological insulators [7,8] that could replace standard transistor-based switching components. Another idea is to leverage topologically protected spin-locked states as a basis for memory in spintronics [9]. Finally, topological insulators and superconductors [10] have been proposed as a basis for quantum computing [11]. With all of these possible applications at stake, it is clearly imperative that we maximize our ability to design and control topological phases of matter.

Consequently *Floquet engineering* [12], where systems are governed by a Hamiltonian possessing dynamic periodicity, has emerged as a promising candidate for precise tuning of topology through the laser-matter interaction. Floquet engineering has already been used both to emulate the Thouless pump with quantized energy as opposed to charge [13,14], and as a method to create novel topological phases from initially trivial phases [15–20]. The recent growth in this field is due to advances in experimental capabilities and theoretical understanding [21–25] in the field of laser-driven quantum mechanics. Much work has been done, particularly in one-dimensional (1D) systems to observe nontrivial phases and transitions of Floquet engineering [26–32]. One powerful theoretical tool in the field of driven lattice systems [33] establishes a mapping of the dynamic D-dimensional system to a static $(D+1)$-dimensional system, in which the modes of the Fourier expansion play the role of lattice points in the new direction. An intriguing feature of the mapping is the emergence of a frequency-dependent field along the new frequency space direction—arising uniquely from the time derivative in the Schrödinger equation. This field dictates the method of solution to be employed. In the case of adiabatic driving where the driving frequency is small as the period $T \to \infty$, the frequency-dependent field is negligible or perturbative, and translational invariance along the frequency direction is assumed. For example, an adiabatically driven 1D Hamiltonian may be mapped to a 2D static representation, where the Floquet-Bloch [33] formalism allows for standard calculations of the Chern number [34,35] to classify the topology. Alternatively in the high-frequency regime, couplings between neighboring Fourier modes become perturbative with the unperturbed Hamiltonian being a time-derivative operator [36]. In the intermediate-frequency region, because the energy scales of the new field and the static Hamiltonian are comparable, approaches beyond perturbation theory should be employed.

In this paper, we study the topological properties of a system driven by two distinct frequencies in the adiabatic and intermediate frequency regimes. Floquet engineering is often employed for a single-frequency drive, with multifrequency (MF) cases being studied more recently [14,37–39]. Broadly speaking, there are two options within the MF formalism: frequencies with (i) commensurate [40] and (ii) incommensurate [41] relationships. The formalism of incommensurate multifrequency driving demands the introduction of a Fourier manifold for each additional drive [41], which has yielded useful application for zero-dimensional qubit frequency mixers [42]. However, this formalism and computation could be

*solin1@binghamton.edu
†wlee@binghamton.edu

cumbersome for two-dimensional systems and above. Moreover, the results in the Floquet formalism rely on truncation of the typically infinite-dimensional Fourier mode space. Two competing truncation methods for a two-tone incommensurate drive may cause complications. Commensurate driving, on the other hand, has already been employed in a variety of situations with great experimental impact. The topology of 1D lattice systems under commensurate driving has been studied before to examine topology, the quality of localization in edge modes, and phase transitions [14,37,38,43]. Another example is commensurate frequency driving being used to create quantum destructive interference in a Fermi-Hubbard model to suppress heating effects [44], which is a prevalent problem in all of Floquet engineering. Finally two-tone drives have been used to engineer nontrivial band structures [45,46].

We employ the commensurate frequency framework developed in [37] to express the MF Floquet formalism using a single period, and we apply this drive to the Su-Schreiffer-Heeger (SSH) model. Note that single-frequency driven SSH variations have already generated great interest in the field [29,30,47,48]. In the adiabatic driving scheme, we map the commensurate drives to the frequency space, resulting in the emergence of new couplings. Careful tuning of the frequencies would allow for simulating nontrivial couplings. To demonstrate this, we explore effects such as next-nearest-neighbor Floquet hopping and large-lattice hopping with two larger, close-by frequencies. The latter effect motivated our interest in this study as a potential temporal analog to the moiré pattern observed in twisted bilayer graphene [49]. Finally, we demonstrate that the dual frequency drive provides an experimentally appealing method for creating a topological phase transition. The different topological regions are simply reached through varying the amplitude mixture.

In simulating the model, we find that standard computational approaches to topology can be troublesome in the presence of the frequency-dependent field originating in the intermediate frequency regime. We address this by employing a real-space variant of the Chern number, called the local Chern marker [50]. Additionally, the Chern marker does not rely on the k-space formulation for the Berry curvature, thus it is more appropriate than neglecting the frequency-field and assuming nonphysical periodic boundaries along the fictitious Fourier manifold. This method allows for visualization of the effect of open boundaries, disorder, and external electromagnetic fields on the topology locally.

II. MODEL

A static Su-Schreiffer-Heeger (SSH) model is known to possess a dimer-type lattice with atoms A, B forming the members of each dimer, and it is topologically nontrivial provided that the intercell coupling is stronger than the intracell coupling. To demonstrate the consequences of multifrequency driving, we consider a Floquet Su-Schreiffer-Heeger (FSSH) model with timevarying, two-frequency tunneling coefficients. The Hamiltonian is kept similar to previous works [51,52] to ensure that upon relaxing the two-drive condition to a single drive, we recover well-established results,

$$H(t)=\sum_{n}^{N} U_1(t)\hat{c}^{\dagger}_{n,B}(t)\hat{c}_{n,A}(t)+U_2(t)\hat{c}^{\dagger}_{n+1,A}(t)\hat{c}_{n,B}(t)V_A(t)\hat{c}^{\dagger} \times_{n+1,A}(t)\hat{c}_{n,A}(t)+V_B(t)\hat{c}^{\dagger}_{n+1,B}(t)\hat{c}_{n,B}(t)+\text{H.c.} \quad (1)$$

In Eq. (1), $U_1(t), U_2(t)$ are the intracell and intercell tunneling strengths, respectively, which are periodic in T. Additionally, we consider the next-nearest-neighbor coupling terms $V_A(t), V_B(t)$. Pulse schemes such as these may be realizable in the cold-atom systems [28,29,53] as noted by several authors [28,30,51,52]. The real-space coordinate can have a periodic boundary condition ($N+1=1$) or an open boundary. The tunneling coefficients

$$\begin{aligned} U_1(t) &= u[1+2(\cos\Omega_1 t+\alpha\cos\Omega_2 t)],\\ U_2(t) &= u[1-2(\cos\Omega_2 t+\alpha\cos\Omega_2 t)],\\ V_A(t) &= v[\cos(\Omega_1 t+\theta)+\alpha\cos(\Omega_2 t+\theta)],\\ V_B(t) &= v[\cos(\Omega_1 t-\theta)+\alpha\cos(\Omega_2 t-\theta)] \end{aligned}$$

are dynamical with driving frequencies $\Omega_{1,2}$ and tunneling amplitudes u, v for the nearest- and next-nearest-neighbor hopping, respectively. The Ω_2 driving factor possesses an "offset" amplitude α, the consequences of which will be discussed in Sec. III.

A. Dual-frequency driving

Here we outline the treatment of Eq. (1) in which the sources are periodic in T_1 and T_2 and are subject to the following condition:

$$\frac{T_1}{T_2}=\frac{n_2}{n_1} \quad (2)$$

for $\{n_1, n_2\} \epsilon \mathbb{Z}^+$, meaning that we may always find [37] a period, T, such that

$$T=n_1T_1=n_2T_2, \quad (3)$$

which may be used to employ the Floquet theory. Note that $\Omega_{1,2}=\frac{2\pi}{T_{1,2}}$. The Hamiltonian may be expressed in terms of components for each period,

$$H(\mathbf{r},t)=H_0+H^{T_1}(\mathbf{r},t)+H^{T_2}(\mathbf{r},t), \quad (4)$$

where the components have the following periodicity: $H^{T_1(T_2)}[\mathbf{r},t+T_1(+T_2)]=H^{T_1(T_2)}(\mathbf{r},t)$, and the system has $H^{T_1(T_2)}(\mathbf{r},t+T)=H^{T_1(T_2)}(\mathbf{r},t)$. The H_0 term is the undriven Hamiltonian. It is important to note that the period of the system is T and so Floquet theory is employed on T, not on either T_1 or T_2. Due to this condition, the derivation of the Floquet Hamiltonian, $\mathcal{K}$, is the same as in the single-frequency case. The single-frequency Floquet Hamiltonian has been derived many times, so we refer the reader to Refs. [12,54]. The general procedure is as follows: from the time-dependent Schrödinger equation $H(t)|\psi(t)\rangle = i\hbar\partial_t|\psi(t)\rangle$, with periodic Hamiltonian $H(t)=H(t+T)$, express the eigenstates as Floquet states that are composed of a nonperiodic phase factor and a T-periodic function: $|\psi(t+T)\rangle = e^{-i\epsilon_\alpha t/\hbar}|\phi_\alpha(t)\rangle$. The factor ϵ_α is the so called

quasienergies named in analogy to the quasimomenta of the familiar Bloch theorem. Then expand the states using a Fourier expansion that moves the time dependence to the phase: $|\phi_\alpha(t)\rangle = \sum_m e^{-im\Omega t}|\phi_\alpha^m\rangle$. Note that the $|\phi_\alpha^m\rangle$'s are Fourier coefficients, which must be stacked up to form the overall Floquet state (for more details, see Ref. [54]). The single-frequency case diverges from the dual-frequency case as we take the expansion in terms of the components of Eq. (4). The components are written in Eq. (5),

$$\mathcal{K} = (H^{T_1}(\mathbf{r},t) + H^{T_2}(\mathbf{r},t)) - i\frac{\partial}{\partial t}. \tag{5}$$

The Fourier expansion on the Floquet modes is then substituted into Eq. (5),

$$(H^{T_1}(\mathbf{r},t) + H^{T_2}(\mathbf{r},t))\sum_m e^{im\Omega t}\left|\phi_\alpha^m\right\rangle + \sum_m m\Omega e^{im\Omega t}\left|\phi_\alpha^m\right\rangle = \epsilon_\alpha \sum_m e^{im\Omega t}\left|\phi_\alpha^m\right\rangle$$

meaning that the matrix elements of Eq. (5), given by the universal equation $\langle\alpha,n|\cdots|\beta,m\rangle = 1/T\int_0^T dt\cdots$, may be computed in the usual way. However, we must consider each new hopping term emerging from each commensurate frequency,

$$\sum_{m,n}\int_0^T dt H^{T_1}(\mathbf{r},t)e^{i\Omega t(m-n)} + \int_0^T dt H^{T_2}(\mathbf{r},t)e^{i\Omega t(m-n)} = \epsilon_\alpha - m\Omega\delta_{m,n},$$

resulting in

$$\sum_{m,n}\left(H^{T_1}_{(m-n)} + H^{T_2}_{(m-n)}\right)\left|\phi_\alpha^m\right\rangle + m\Omega\delta_{m,n}\left|\phi_\alpha^m\right\rangle = \epsilon_\alpha\left|\phi_\alpha^n\right\rangle, \tag{6}$$

where $H^{T_1(T_2)}_{(m-n)} = \frac{1}{T}\int_0^T dt H^{T_1(T_2)}(\mathbf{r},t)e^{i\Omega t(m-n)}$, and the ϵ_α eigenvalues are the quasienergies of the system. Note that the Fourier factor $e^{i\Omega t(m-n)}$ is left in Ω, the frequency of the system, not in either Ω_1 or Ω_2. The result of mapping our Hamiltonian to the static 2D version is shown in Fig. 1. We now discuss the terms in Eq. (6). Note the effective field $m\Omega$ appearing in the 2D representation is a consequence of the time derivative in Eq. (5). This field, commonly denoted as the "Stark field," [12,54–56] may be considered as a fictitious electric field emerging along the Fourier manifold. The energy scale $\hbar\Omega$ often dictates the solution. With adiabatic (slow, long-time) driving ($T\to\infty, \Omega\to 0$), the scale is set by the couplings $m\hbar\Omega \ll H^{T_1,T_2}_{m-n}$, which emerge from new frequencies added in the drive. The coupling factor in the Floquet Hamiltonian in Eq. (6) compared to the single-frequency case reveals that multimode theory with commensurate drives allows for construction of new kinetic terms. One may expect a new coupling for each commensurate drive added. Careful construction of these new frequencies may yield exotic new physics, or open the route for Floquet systems to mimic the physics of some experimentally intractable static systems in condensed matter.

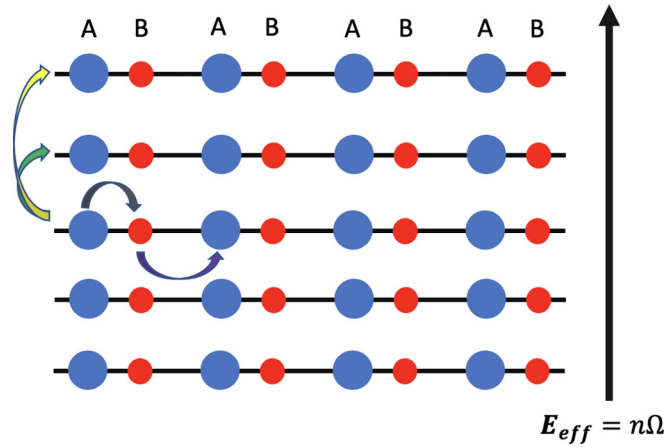

FIG. 1. 2D Static Floquet SSH representation. In gray: intracell hopping, purple: intercell hopping, green: nearest-neighbor Floquet (NNF) hopping, yellow: next-nearest-neighbor Floquet (NNNF) coupling. The basic couplings are shown, but the Hamiltonian allows for any combination, e.g., NNNF+intercell off-diagonal element is present in H.

III. RESULTS

The Hamiltonian [Eq. (1)] is constructed for atoms A, B with 20 dimers, resulting in 40 real-space matrix elements. We set $u = 1, v = 0.2, \theta = 0.5\pi, \alpha = 2$ unless otherwise stated. We employ the multifrequency Floquet theory [Eq. (6)] to map the time-dependent 1D system to the static 2D enlarged space (Fig. 1). Provided that the driving is adiabatic ($m\hbar\Omega \ll H^{T_1,T_2}_{m-n}$), it is common [51,52] to assume a periodic boundary condition along the Fourier space and subsequently define a Floquet quasimomentum k_f. The frequency is taken as small as possible to ensure adiabaticity, but large enough for measurement [51]. However, we argue that the approximation is not ideal because (i) the driving frequency cannot be neglected, thus breaking Fourier-space translational invariance, and (ii) there is no physical operator connecting the largest and smallest cutoff frequencies of the expansion. We therefore leave the system in the real-space matrix form. While this matrix is technically infinite, we can study a truncated space using the Chern marker to examine the topological order [54,57]. We consider 200 Floquet modes, m, resulting in an 8000×8000 matrix unless otherwise stated, which we construct and diagonalize in FORTRAN. All presented calculations of the Chern number are accurate up to a maximum error of 1%. Where stated, the Stark field is considered by adding in the $m\Omega$-dependent value along the Floquet diagonal δ_{nm}. As for the coupling, the integers chosen in Eq. (2) result in different δ functionals after integration of Eq. (6) in the Floquet space due to the cosine drive. For example, $n_1 = 10 \to \delta_{n,m+10} + \delta_{n,m-10}$. Although theoretically any integer ratio may be employed, here we consider the $\{n_1, n_2\}$ cases of $\{1,1\}$ (single-drive reference), $\{1,2\}$ (Floquet next-nearest neighbor), and $\{10,11\}$ (close-by beat frequency).

A. Topology—Single drive

Our model relaxes to a single-drive case by setting $\alpha = 0$, and setting Ω_1 as the base frequency. In Fig. 2, we plot the

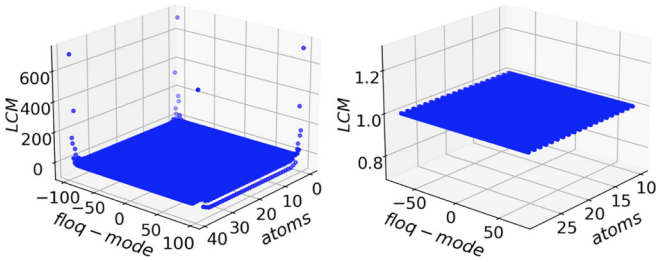

FIG. 2. Two plots of the Chern marker in the case $\Omega \to 0$. Left is the Chern marker over the whole system, in two dimensions, real space, and Floquet space. The average Chern number is 0, due to the trace identity [50]. In the region away from the edge as shown in the right plot, we obtain a Chern marker of 1, corresponding to the bulk topology. The marker is stable in the bulk, and nonphysical near the edges.

Chern marker over the static 2D representation of the sample in the presence of periodic boundaries. As expected [50], averaged over the entire sample the marker is 0 due to its commutator definition. However, in the bulk of the sample, the average Chern marker yields 1, in excellent agreement with the Fukui method. Previous works [52] have discovered that the single-drive Hamiltonian is topologically nontrivial for nonzero θ. However, these predictions enforce translationally invariant samples and rely on computational methods using k-space, meaning the effect of the Stark field on the topological order is ignored. By employing the local Chern marker [50], we provide both real-space confirmation of single-drive topology, and simple determination of topology in the face of the Stark electric field. An advantage of computing topology using the Chern marker is that we may easily reintroduce the Stark field along the frequency direction for small values of Ω. Consequently, the topology may be visualized along each direction in response to increasing field value, or even disorder along the real-space direction. In Fig. 3, we plot the Chern marker along real and frequency space with increasing Stark electric field $\propto \Omega$. We see the real-space Chern marker unaffected everywhere by increasing Ω. Similarly, for finite but small Ω the frequency space Chern marker remains unaffected. However, as Ω increases, the LCM along the frequency space does not remain topologically invariant and the system does not have a meaningful topology. At the very center of the sample where $m = n \approx 0$, the expected topology is recovered, which is consistent with the adiabatic theorem for small fields ($m\Omega$). Consequently, this calculation may be used to probe maximum allowed values of Ω above which the topology becomes ill-defined.

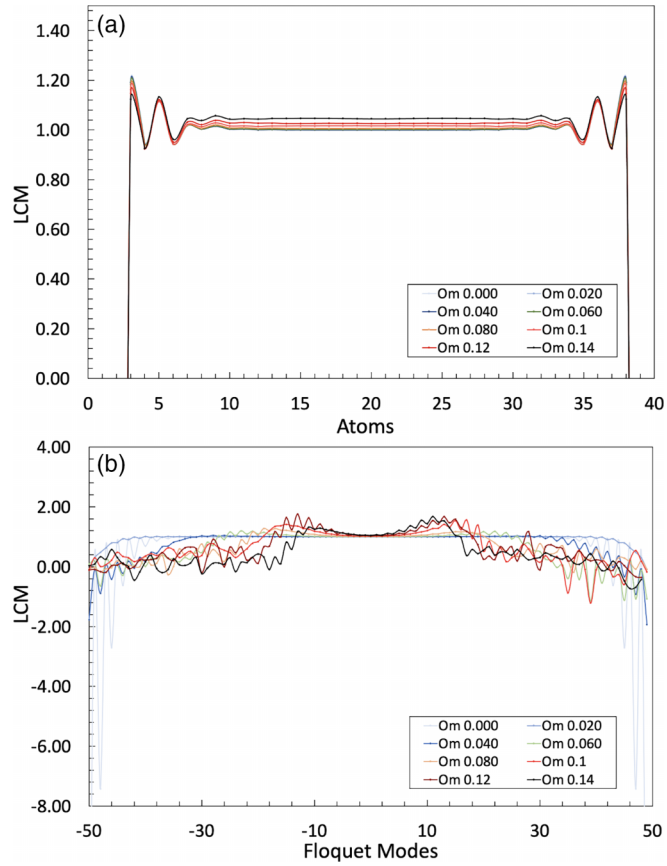

FIG. 3. Chern marker plotted in (a) real space and (b) Floquet space, for increasing Ω, the magnitude of the Stark field. Note that only 100 Floquet modes were used. In (a) the real-space Chern marker is not strongly changed by increasing Ω—a sensible result as the Stark field only permeates the Floquet space. In (b) the Stark field destroys the topological order in the sample as Ω increases, but notice that for small m the Chern marker returns to the expected Chern number of 1, confirming the adiabatic theorem for small Ω.

B. Multifrequency drive: Case 1,2

1. *Topological phase transition*

We examine the effects of the second drive for the frequency ratio $n_1, n_2 = 1, 2$. This ratio has been studied before for a variety of systems, including 1D chains [14,37,38,43–46]. The band structure and the Chern marker under periodic boundaries in each direction (adiabatic driving $\Omega \to 0$, translational invariance along the Fourier manifold) are computed and shown in Fig. 4. The interpretation of this model is the presence of a next-nearest-neighbor coupling along the frequency space. The system still possesses a gap for $n_1, n_2 = 1, 2$, but only when the two drives have a difference in amplitude are different. Here we fix $\alpha = 2$. Due to the invariance,

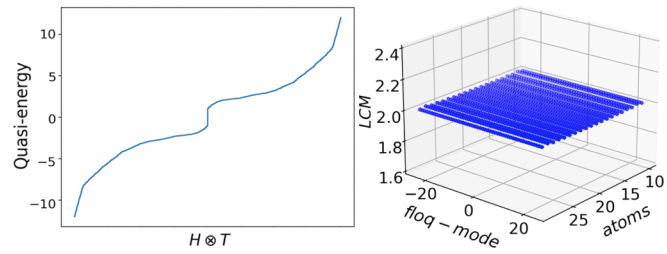

FIG. 4. The band (left) and Chern marker interior (right) for the case $n_1 = 1$, $n_2 = 2$, and $\Omega \to 0$. This case simulates a second-neighbor hopping in the Floquet space—impossible to achieve without a second drive. The system is found to be insulating with a quasienergy gap of $\sim$2.0, meaning topology can be computed. The right plot shows the interior of the Chern marker, and the bulk average value of 2.

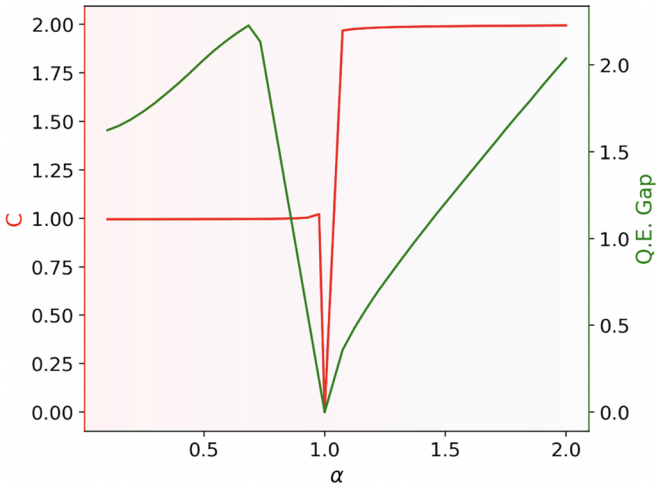

FIG. 5. The Chern number in red plotted against the Ω_2 driving amplitude α for the case $\Omega \to 0$. Note that the amplitude on Ω_1 is 1. Below the transition point 1, the Chern number is robustly 1. Above the transition point, the Chern number is robustly 2. The quasienergy gap is shown to close at the transition point in green. The color gradient is shown to signify that even changing parameters such as θ, u, v will yield the same results provided that the gap is not closed.

the Chern marker is seen to be relatively stable with little variation over the sample bulk. We find that the Chern number is 2, indicating that an advantage of commensurate driving is the ability to engineer phases with $C > 1$. Surprisingly, we discover that the offset amplitude between the drives functions as a tuning parameter for a topological phase transition (TI). This transition is plotted in Fig. 5. For $\alpha < 1$, $C = 1$, and for $\alpha > 1$, $C = 2$. The transition occurs through the gap closing condition of $\alpha = 1$. Note that the gap is computed as the difference between the lowest conduction-band and highest valence-band quasienergies. The gap closes on Brillouin zone corners $\{k_x, k_f\} = \{-\pi, -\pi\}$, etc., but initially the smallest difference is elsewhere in the Brillouin zone. This transition is not unique to the case of $n_1, n_2 = 1, 2$. We expect this behavior for any choice of Ω_1, Ω_2 provided that the system remains gapped. The Chern number will transition with the amplitude mixture controlling the critical point, and the frequencies controlling the topology. This amplitude modulation of a two-frequency drive should be experimentally feasible. It does not rely on fabrication of the lattice or on a quantum-well thickness [58]. The current formalism presents an easily tunable topological phase transition, based simply on the control of the driving lasers. However, it is also known [46] that the relative phase of the two-frequency drive can change the symmetry of the system, which is being examined in ongoing calculations.

2. Edge states

The topology present in this drive case has an observable physical effect, manifested in the emergence of edge modes (states that have a nonzero wave function only along the boundary of a sample) along the edges of the effective 2D sample. In Fig. 6 we plot the zero-quasienergy eigenstates upon opening both the Floquet and the real-space

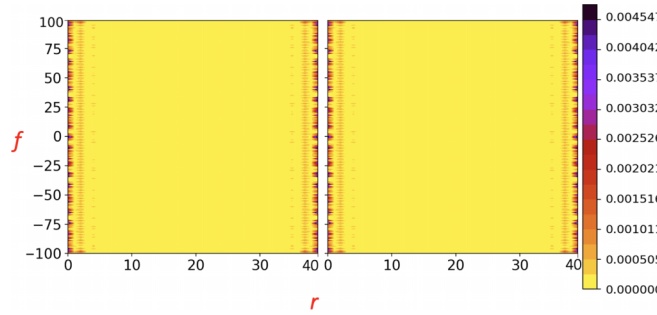

FIG. 6. Edge modes occurring along the real-space edge in the case $\Omega \to 0$, and $n_1, n_2 = 1, 2$ driving frequency ratio. The contour is computed for $\psi^\dagger \psi_{i,j}$, for i, j the real and frequency space, respectively. The states plotted are the zero-quasienergy states.

boundary. The states are seen in Fig. 6 to occupy the real-space boundary, with amplitude diminishing to 0 in the center of the sample. This plot is constructed by taking $\psi^\dagger \psi_{i,j}$ for i, j, the real and frequency space elements, respectively, for the eigenstates at zero-quasienergy. The real-space treatment easily allows us to plot the zero-quasienergy states for a variety of boundary conditions. For example, one may reinstate translational invariance along the SSH chain, break invariance of the Fourier manifold, and recompute the amplitude of 6. In this case, we find that the edge states exist along the "Fourier edge" only. Unlike SSH chain edge states, which may be observable in current measurements, Fourier edges are only an artifact of the theoretical Floquet mapping and subsequent truncation scheme, so we neglect the result in the current paper.

C. Multifrequency drive: Case 10,11

1. Exotic topology

Here we examine the effects of the second drive in the case of frequency ratio $n_1, n_2 = 10, 11$. The band structure and the Chern marker for the case of periodic boundaries in each direction are computed and plotted in Fig. 7. The system possesses a gap for $n_1, n_2 = 10, 11$, with condition $\alpha = 2$. The Chern marker is seen to be not as stable over the sample bulk as in the $n_1, n_2 = 1, 2$ case, resulting from interference between the two close-by frequencies. We again tune α through

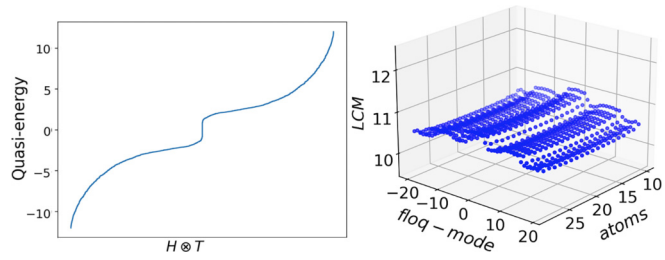

FIG. 7. The band and Chern marker interior for the case $n_1 = 10$, $n_2 = 11$, and $\Omega \to 0$. The band is shown in the left, and the system is found to be gapped in quasienergy, meaning topology can be computed. The right plot shows the interior of the Chern marker, and the bulk average value of 11. Note that the $n_1, n_2 = 10, 11$ shows more interference in the LCM than the 1,2 case.

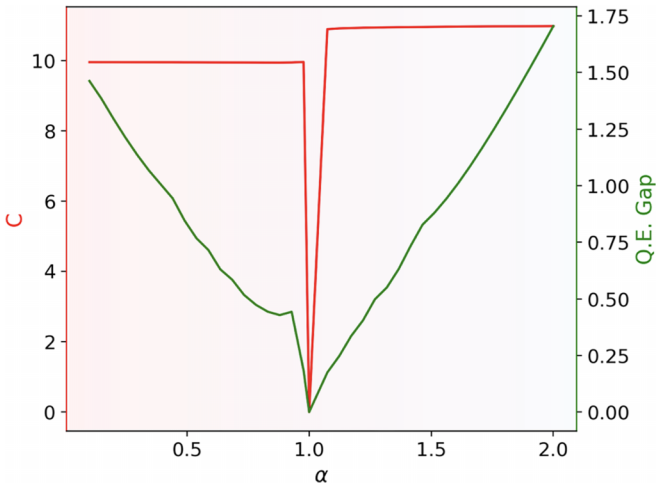

FIG. 8. The Chern number in red plotted against the Ω_2 driving amplitude α in the case $\Omega \to 0$. Note that the amplitude on Ω_1 is 1. Below the transition point 1, the Chern number is robustly 10. Above the transition point, the Chern number is robustly 11. The quasienergy gap closes at the transition point of $\alpha = 1$. The color gradient is shown to signify that even changing parameters such as θ, u, v will yield the same results provided that the gap is not closed.

the critical point, as plotted in Fig. 8. The system displays the same phase-transition behavior as in the $n_1, n_2 = 1, 2$ case. The Chern number is found to be $C = 10$ for $\alpha < 1$ and $C = 11$ for $\alpha > 1$. Our motivation in studying the multifrequency driving was to model a beat frequency Hamiltonian. This is based on the hope that the disorder induced by the beat frequency along the Floquet direction would be a temporal analog to the twisted bilayer graphene, in which maximum disorder occurs for certain "magic" angles. The requirement, therefore, is that the two drives possess frequencies that are close in value. The size of the matrix must accommodate long-range couplings. The case for $n_1, n_2 = 10, 11$ is explored using our current FORTRAN code, but larger frequency ratios like 100,101 demand a much larger matrix. This larger case would be ideal to consider for the beat frequency analog.

2. Edge states

Since the system still possesses topological order, we can plot edge modes by opening the sample boundaries. We plot the zero-energy states in the case of broken periodic boundaries in each case. This result is shown in Fig. 9. Again as in the $n_1, n_2 = 1, 2$ case we find states existing along the real-space edge only. As noted in the case of $n_1, n_2 = 1, 2$, we also may break translational invariance along the Fourier space. In this case, the amplitude is only nonzero for certain modes along the Fourier manifold, as opposed to the modes at the very "edge." The presence of mode-localized states could be an artifact of the truncation scheme, so their effect is best seen in defining and computing a physical observable in the 1D time-dependent model.

IV. DISCUSSION

A. Multitonal driving—Integer multiples

There are, broadly speaking, three contrasting multitonal driving cases for which the Floquet formalism may be

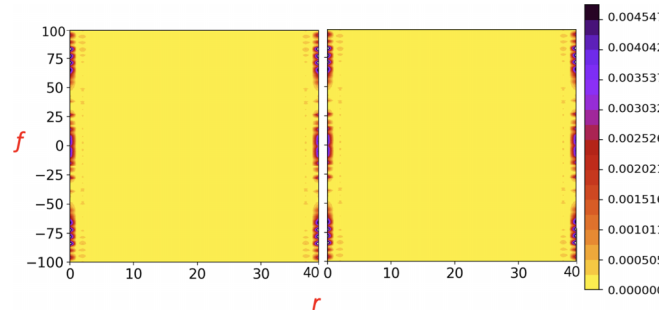

FIG. 9. Edge modes occurring along the real-space edge in the case $\Omega \to 0$ and $n_1, n_2 = 10, 11$ driving frequency ratio. The contour is computed for $\psi^\dagger \psi_{i,j}$, for i, j the real and frequency space, respectively. The states plotted are the zero-quasienergy states.

constructed. The simplest is when the frequencies are not only commensurate but related via integer multiple. Examples for $\Omega_2/\Omega_1 = n_1/n_2$ are $n_1, n_2 = 2, 4$ or $n_1, n_2 = 1, 3$. In this case, one frequency may be determined in terms of the other. The relative phase of the drives plays a critical role, as explored in recent works [44–46]. The formalism of Eq. (2) is unnecessary for this driving protocol. In fact, constructing the formalism in terms of the base period may yield incorrect computation of observables. For example, treating $n_1, n_2 = 2, 4$ with a base frequency with $n = 1$ will encode an extra integer lattice spacing, yielding new nonphysical twisting in the Berry curvature from $\vec{k} \to \vec{k} + d\vec{k}$. For example, the computation of the transition would yield $C = 2 \to C = 4$ when it is physically $C = 1 \to C = 2$.

B. Multitonal driving—Commensurate and incommensurate

On the other hand, there is another sort of commensurate two-tone drive where the integers cannot be uniquely expressed via an integer multiple, such as $n_1, n_2 = 4, 5$ or $n_1, n_2 = 10, 11$. The Floquet theorem and topology of this case may be studied with the formalism of [37], and the topology may be computed using the frequency-space Chern marker presented here. This treatment follows from the fact that the time degree of freedom should have a one-to-one correspondence with the Fourier transform to the extended space. The Floquet lattice obtains new couplings computed from the off-diagonal matrix elements of Eq. (5). This case is distinguished from the incommensurate frequency driving [41] in which each frequency yields an additional Fourier manifold. To treat the 1D SSH in this case would require a 3D computation. Additionally, two truncation schemes of the Fourier space are needed. It could be advantageous to approximate certain incommensurate ratios with nearby commensurate ones and carry out the simpler calculations presented here.

C. Floquet edge states

Upon opening the "Fourier boundary," we find the zero quasienergy modes localized to the truncation edge in the case of $n_1, n_2 = 1, 2$, and localized to certain frequencies in the case of $n_1, n_2 = 10, 11$. Since the Fourier boundary physically does not exist, it is simply an artifact of the theoretical mapping; these results are neglected as byproducts of the

frequency truncation. The distinction between the two cases (one edge-localized and one mode-localized) could arise from the fact that the matrix size stays the same, but for higher frequencies the kinetic terms populate even further off-diagonal elements. In other words, increasing the cutoff may cause the mode-localized states to shift to the edges. While the Floquet edge is nonphysical, it is possible to break periodic boundary conditions along the Fourier manifold with a small Stark field. The consequences are best observed in this case by computing observables such as current in the original time-dependent representation.

V. CONCLUSIONS

In this paper, we have shown that the commensurate multifrequency driving formalism may be modeled using the Fourier mapping of Floquet theory to gain practical levels of engineering control. The frequency ratio may be chosen to create new couplings, which allows the Floquet formalism to mimic difficult static systems. We find that a second commensurate drive amounts to an extra hopping term in the Fourier manifold. This approach necessitates only one Fourier manifold extension, meaning that commensurate driving can be studied easily in one- and two-dimensional systems. Finally, only one truncation scheme is needed in the extended space as opposed to two or more for incommensurate driving.

To explore the topological properties, we have employed the real-space Chern marker instead of the Berry curvature in k-space representation, which allows us to study the adiabatic and intermediate frequency regimes using the same framework. The model can incorporate disorder and fields, more closely approximating a real system. This approach yields direct examination of the local fluctuations in topology resulting from interference, and of the edge states. Moreover, our work provides a method for controlling the topological phase of an SSH sample, and an appropriate choice of the frequency ratio allows for engineering of Chern numbers $C > 1$. Consequently, the amplitude proportion of the two drives may be tuned to induce topologically distinct states, meaning that these systems can be engineered to sweep through a topological phase transition. Since these topological phases are induced via the amplitude, this model hosts an experimentally appealing transition that does not rely on a switching mechanism such as in the quantum wells. We have further demonstrated a computation technique to view edge states in the insulating phase, providing additional confirmation that these systems are topological insulators.

ACKNOWLEDGMENTS

This work was supported by the Air Force Office of Scientific Research Multi-Disciplinary Research Initiative (MURI) entitled "Cross-disciplinary Electronic-ionic Research Enabling Biologically Realistic Autonomous Learning (CEREBRAL)" under Award No. FA9550-18-1-0024 administered by Dr. A. Sayir. S.O. and W.-C.L. are grateful for the support of the summer faculty fellowship program (SFFP) sponsored by the Air-Force-Research-Lab (AFRL) while this paper was being finalized.

[1] K. v. Klitzing, G. Dorda, and M. Pepper, New Method for High-Accuracy Determination of the Fine-Structure Constant Based on Quantized Hall Resistance, Phys. Rev. Lett. **45**, 494 (1980).

[2] M. V. Berry, Quantal phase factors accompanying adiabatic changes, Proc. R. Soc. London A **392**, 45 (1984).

[3] D. J. Thouless, M. Kohmoto, M. P. Nightingale, and M. den Nijs, Quantized Hall Conductance in a Two-Dimensional Periodic Potential, Phys. Rev. Lett. **49**, 405 (1982).

[4] F. D. M. Haldane, Model for a Quantum Hall Effect without Landau Levels: Condensed-Matter Realization of the "Parity Anomaly," Phys. Rev. Lett. **61**, 2015 (1988).

[5] W. P. Su, J. R. Schrieffer, and A. J. Heeger, Soliton excitations in polyacetylene, Phys. Rev. B **22**, 2099 (1980).

[6] *International Roadmap for Devices and Systems (IRDS™)* (IEEE, Piscataway, NJ, 2018).

[7] C. Yue, S. Jiang, H. Zhu, L. Chen, Q. Sun, and D. W. Zhang, Device applications of synthetic topological insulator nanostructures, Electronics **7**, 225 (2018).

[8] M. J. Gilbert, Topological electronics, Commun. Phys. **4**, 70 (2021).

[9] L. Šmejkal, Y. Mokrousov, B. Yan, and A. H. MacDonald, Topological antiferromagnetic spintronics, Nat. Phys. **14**, 242 (2018).

[10] M. Leijnse and K. Flensberg, Introduction to topological superconductivity and majorana fermions, Semicond. Sci. Technol. **27**, 124003 (2012).

[11] G. Scappucci, P. J. Taylor, J. R. Williams, T. Ginley, and S. Law, Crystalline materials for quantum computing: Semiconductor heterostructures and topological insulators exemplars, MRS Bull. **46**, 596 (2021).

[12] T. Oka and S. Kitamura, Floquet engineering of quantum materials, Annu. Rev. Condens. Matter Phys. **10**, 387 (2019).

[13] M. H. Kolodrubetz, F. Nathan, S. Gazit, T. Morimoto, and J. E. Moore, Topological Floquet-Thouless Energy Pump, Phys. Rev. Lett. **120**, 150601 (2018).

[14] Y. Pan, A. Dikopoltsev, E. Lustig, Q. Cheng, and M. Segev, Anomalous floquet thouless pumping, in *2021 Conference on Lasers and Electro-Optics (CLEO)* (IEEE, Piscataway, NJ, 2021), pp. 1–2.

[15] M. S. Rudner, N. H. Lindner, E. Berg, and M. Levin, Anomalous Edge States and the Bulk-Edge Correspondence for Periodically Driven Two-Dimensional Systems, Phys. Rev. X **3**, 031005 (2013).

[16] N. H. Lindner, G. Refael, and V. Galitski, Floquet topological insulator in semiconductor quantum wells, Nat. Phys. **7**, 490 (2011).

[17] L. Jiang, T. Kitagawa, J. Alicea, A. R. Akhmerov, D. Pekker, G. Refael, J. I. Cirac, E. Demler, M. D. Lukin, and P. Zoller, Majorana Fermions In Equilibrium And In Driven Cold-Atom Quantum Wires, Phys. Rev. Lett. **106**, 220402 (2011).

[18] T. Oka and H. Aoki, Photovoltaic hall effect in graphene, Phys. Rev. B **79**, 081406(R) (2009).

[19] T. Kitagawa, T. Oka, A. Brataas, L. Fu, and E. Demler, Transport properties of nonequilibrium systems under the application of light: Photoinduced quantum hall insulators without landau levels, Phys. Rev. B **84**, 235108 (2011).

[20] Y. T. Katan and D. Podolsky, Modulated Floquet Topological Insulators, Phys. Rev. Lett. **110**, 016802 (2013).

[21] J. B. Delos, Theory of electronic transitions in slow atomic collisions, Rev. Mod. Phys. **53**, 287 (1981).

[22] N. L. Manakov, V. D. Ovsiannikov, and L. P. Rapoport, Atoms in a laser field, Phys. Rep. **141**, 320 (1986).

[23] A. Fainshtein, N. Manakov, V. Ovsiannikov, and L. Rapoport, Nonlinear susceptibilities and light scattering on free atoms, Phys. Rep. **210**, 111 (1992).

[24] S.-I. Chu and D. A. Telnov, Beyond the floquet theorem: generalized floquet formalisms and quasienergy methods for atomic and molecular multiphoton processes in intense laser fields, Phys. Rep. **390**, 1 (2004).

[25] K. Nasu, *Photoinduced Phase Transitions* (World Scientific, Singapore, 2004).

[26] Q. Cheng, Y. Pan, H. Wang, C. Zhang, D. Yu, A. Gover, H. Zhang, T. Li, L. Zhou, and S. Zhu, Observation of Anomalous π Modes in Photonic Floquet Engineering, Phys. Rev. Lett. **122**, 173901 (2019).

[27] A. Xie, S. Zhou, K. Xi, L. Ding, Y. Pan, Y. Ke, H. Wang, S. Zhuang, and Q. Cheng, Nonparaxiality-triggered landau-zener transition in spoof plasmonic waveguides, Phys. Rev. B **106**, 174301 (2022).

[28] O. Balabanov and H. Johannesson, Robustness of symmetry-protected topological states against time-periodic perturbations, Phys. Rev. B **96**, 035149 (2017).

[29] V. Dal Lago, M. Atala, and L. E. F. Foa Torres, Floquet topological transitions in a driven one-dimensional topological insulator, Phys. Rev. A **92**, 023624 (2015).

[30] A. Agrawal and J. N. Bandyopadhyay, Floquet topological phases with high chern numbers in a periodically driven extended su–schrieffer–heeger model, J. Phys.: Condens. Matter **34**, 305401 (2022).

[31] M. Jangjan and M. V. Hosseini, Floquet engineering of topological metal states and hybridization of edge states with bulk states in dimerized two-leg ladders, Sci. Rep. **10**, 14256 (2020).

[32] M. Jangjan and M. V. Hosseini, Topological phase transition between a normal insulator and a topological metal state in a quasi-one-dimensional system, Sci. Rep. **11**, 12966 (2021).

[33] A. Gómez-León and G. Platero, Floquet-Bloch Theory and Topology in Periodically Driven Lattices, Phys. Rev. Lett. **110**, 200403 (2013).

[34] D. Xiao, M.-C. Chang, and Q. Niu, Berry phase effects on electronic properties, Rev. Mod. Phys. **82**, 1959 (2010).

[35] T. Fukui, Y. Hatsugai, and H. Suzuki, Chern numbers in discretized brillouin zone: Efficient method of computing (spin) hall conductances, J. Phys. Soc. Jpn. **74**, 1674 (2005).

[36] A. Eckardt and E. Anisimovas, High-frequency approximation for periodically driven quantum systems from a floquet-space perspective, New J. Phys. **17**, 093039 (2015).

[37] P. Molignini, Edge mode manipulation through commensurate multifrequency driving, Phys. Rev. B **102**, 235143 (2020).

[38] J. Naji, R. Jafari, L. Zhou, and A. Langari, Engineering floquet dynamical quantum phase transitions, Phys. Rev. B **106**, 094314 (2022).

[39] Q. Cheng, H. Wang, Y. Ke, T. Chen, Y. Yu, Y. S. Kivshar, C. Lee, and Y. Pan, Asymmetric topological pumping in nonparaxial photonics, Nat. Commun. **13**, 249 (2022).

[40] A. N. Poertner and J. D. D. Martin, Validity of many-mode floquet theory with commensurate frequencies, Phys. Rev. A **101**, 032116 (2020).

[41] I. Martin, G. Refael, and B. Halperin, Topological Frequency Conversion in Strongly Driven Quantum Systems, Phys. Rev. X **7**, 041008 (2017).

[42] G. Wang, Y.-X. Liu, J. M. Schloss, S. T. Alsid, D. A. Braje, and P. Cappellaro, Sensing of Arbitrary-Frequency Fields Using a Quantum Mixer, Phys. Rev. X **12**, 021061 (2022).

[43] T. Nag, R.-J. Slager, T. Higuchi, and T. Oka, Dynamical synchronization transition in interacting electron systems, Phys. Rev. B **100**, 134301 (2019).

[44] K. Viebahn, J. Minguzzi, K. Sandholzer, A.-S. Walter, M. Sajnani, F. Görg, and T. Esslinger, Suppressing Dissipation in a Floquet-Hubbard System, Phys. Rev. X **11**, 011057 (2021).

[45] K. Sandholzer, A.-S. Walter, J. Minguzzi, Z. Zhu, K. Viebahn, and T. Esslinger, Floquet engineering of individual band gaps in an optical lattice using a two-tone drive, Phys. Rev. Res. **4**, 013056 (2022).

[46] J. Minguzzi, Z. Zhu, K. Sandholzer, A.-S. Walter, K. Viebahn, and T. Esslinger, Topological Pumping in a Floquet-Bloch Band, Phys. Rev. Lett. **129**, 053201 (2022).

[47] C. Borja, E. Gutiérrez, and A. López, Emergence of floquet edge states in the coupled su–schrieffer–heeger model, J. Phys.: Condens. Matter **34**, 205701 (2022).

[48] O. Dmytruk and M. Schirò, Controlling topological phases of matter with quantum light, Commun. Phys. **5**, 271 (2022).

[49] R. Bistritzer and A. H. MacDonald, Moiré bands in twisted double-layer graphene, Proc. Natl. Acad. Sci. (USA) **108**, 12233 (2011).

[50] R. Bianco and R. Resta, Mapping topological order in coordinate space, Phys. Rev. B **84**, 241106 (2011).

[51] J.-Y. Zou and B.-G. Liu, Quantum floquet anomalous hall states and quantized ratchet effect in one-dimensional dimer chain driven by two ac electric fields, Phys. Rev. B **95**, 205125 (2017).

[52] X.-L. Lü and H. Xie, Topological phases and pumps in the su–schrieffer–heeger model periodically modulated in time, J. Phys.: Condens. Matter **31**, 495401 (2019).

[53] M. Lohse, C. Schweizer, O. Zilberberg *et al.*, A thouless quantum pump with ultracold bosonic atoms in an optical superlattice, Nat. Phys. **12**, 350 (2016).

[54] M. S. Rudner and N. H. Lindner, The floquet engineer's handbook Nat. Rev. Phys. **2**, 229 (2020).

[55] L. Privitera, Non-equilibrium aspects of topological Floquet quantum systems, Ph.D. thesis, International School for Advanced Studies, 2017.

[56] G. H. Wannier, Wave functions and effective hamiltonian for bloch electrons in an electric field, Phys. Rev. **117**, 432 (1960).

[57] M. Holthaus, Floquet engineering with quasienergy bands of periodically driven optical lattices, J. Phys. B **49**, 013001 (2016).

[58] B. A. Bernevig, T. L. Hughes, and S.-C. Zhang, Quantum spin hall effect and topological phase transition in HgTe quantum wells, Science **314**, 1757 (2006).